HHS Public Access

Author manuscript

Macromol Biosci. Author manuscript; available in PMC 2019 September 01.

Published in final edited form as:

Macromol Biosci. 2018 September ; 18(9): e1800090. doi:10.1002/mabi.201800090.

Nanofiber-Based Multi-Tubular Conduits with a Honeycomb Structure for Potential Application in Peripheral Nerve Repair

Dr. Jiajia Xue,

The Wallace H. Coulter Department of Biomedical Engineering, Georgia Institute of Technology and Emory University, Atlanta, GA 30332, USA

Haoxuan Li, and

The Wallace H. Coulter Department of Biomedical Engineering, Georgia Institute of Technology and Emory University, Atlanta, GA 30332, USA

Prof. Younan Xia

School of Chemistry and Biochemistry, School of Chemical and Biomolecular Engineering, Georgia Institute of Technology, Atlanta, GA 30332, USA; The Wallace H. Coulter Department of Biomedical Engineering, Georgia Institute of Technology and Emory University, Atlanta, GA 30332, USA

Abstract

Peripheral nerve injury is a large-scale problem and it is a grand challenge to repair the long lesion in a thick nerve. Here we report the design of a multi-tubular conduit with a honeycomb structure by mimicking the anatomy of a peripheral nerve for the potential repair of large defects in thick nerves. A bilayer mat of electrospun nanofibers is rolled up to form a single tube, with the inner and outer layers comprised of aligned and random nanofibers, respectively. Seven such tubes are then assembled into a hexagonal array and encased within the lumen of a larger tube to form the multi-tubular conduit. By introducing an adhesive to the regions between the tubes, the conduit is robust enough for handling during surgery. The seeded bone marrow stem cells (BMSCs) are able to proliferate in all the tubes with even circumferential and longitudinal distributions. Under chemical induction, the BMSCs are transdifferentiated into Schwann-like cells in all the tubes. While the cellular version holds great promise for peripheral nerve repair, the multi-tubular conduit can also be used to investigate the fundamental aspects involved in the development of peripheral nervous system and migration of cells.

Graphical Abstract

A multi-tubular conduit with a honeycomb structure is fabricated by assembling seven small tubes based on electrospun nanofibers into a hexagonal array and wrapped within a larger tube.

younan.xia@bme.gatech.edu.

Conflict of Interest

The authors declare no conflict of interest.

Supporting Information

Supporting Information is available from the Wiley Online Library or from the author.

Bone marrow stem cells are then seeded and transdifferentiated into Schwann-like cells in all the tubes, generating a cellular conduit for potential use in repairing long lesions in thick nerves.

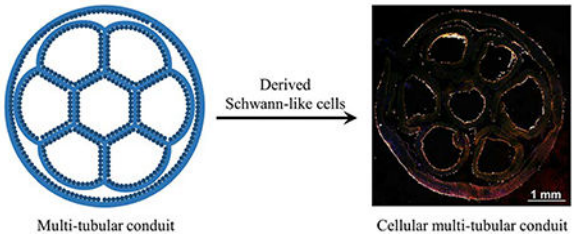

Keywords

multi-tubular conduit; electrospun nanofibers; bone marrow stem cells; Schwann cells; nerve tissue engineering

1 Introduction

Peripheral nerve injury is a large-scale problem that seriously affects the life quality of many patients.[1–3] Due to the limited regeneration capability of the peripheral nervous system, it is desirable to graft a bridge across the lesion. Autografts are the clinical “gold standard” for bridging the peripheral nerve lesions. However, the limited supply of donor nerves makes it difficult to reconstruct complex nerve gaps. To this end, artificial nerve guidance conduits (NGCs) that provide a suitable environment for axon regeneration have been developed. The NGC is often used to bridge the gap between the proximal and distal stumps to enhance the nerve regeneration efficiency.[4–6] The ends of the damaged nerve are inserted into the ends of a conduit, which is typically made of either natural or synthetic biomaterials.[7,8] The conduit acts not only as a connecting bridge for the severed nerve ends but also as a protective sheath for the regenerating nerve.[9]

Among the products that have been approved by the U.S. Food and Drug Administration (FDA), NeuraGen® based on type I collagen and Neurolac® based on polycaprolactone (PCL) are most extensively used in the pre-clinical and clinical settings.[10,11] All these single-tubular conduits, however, have limited capabilities in facilitating axon regrowth and function recovery over long (>2 cm in length) lesions in thick (>2 mm in diameter) nerves because the relatively large hollow lumen cannot recapitulate the anisotropic structure of a nerve and it cannot effectively supply glial cells to support neurite regrowth either.[12,13] Failed clinical outcomes in repairing thick nerves using single-tubular NGCs have been reported.[14] In one case, it was shown that the use of a single-tubular conduit made of polyglycolic acid did not impact the repair of a defect (2 cm in length and 4 mm in diameter) created in ulnar nerve. In another effort involving NeuraGen® (Integra NeuroSciences) type I collagen conduit, no function recovery was observed after 14 months of repair for a nerve defect of 3 cm in length and 4 mm in diameter.

To address the aforementioned issues, conduits with an advanced design have been explored recently. Electrospun nanofibers and hydrogels represent two major classes of materials used to construct the walls of the conduits.[15–17] As a major drawback, conduits made of

hydrogels cannot be easily used for long nerve gaps due to the lack of mechanical integrity under physiological conditions. Swelling of hydrogels has also been shown to close the conduit cavity and thus block axon growth.[16] Owing to the highly porous structures and the ability to collect them as uniaxially aligned arrays, electrospun nanofibers have shown great promise for conduit fabrication.[18–26] The aligned nanofibers can provide a topographical cue to direct and enhance axon extension during regeneration.[23,27–28] However, the repair of thick nerves using single-tubular conduits still remains problematic because the effect of longitudinal guidance gradually weakens from the wall to the center of a large conduit.[29]

Recently, multi-channeled NGCs that mimic the fascicular architecture of a native nerve have been explored to enhance axon extension and to guide directional re-innervation.[12,30–37] Various types of conduits with multiple parallel channels along the length of the conduits have been fabricated using techniques such as injection molding,[30,31] stereolithography,[32] thermally induced phase separation,[33,34] and sacrificial templating approach.[35] The as-fabricated conduits are limited in their abilities to enable effective regeneration because of the lack of topographical guidance cues. Based on uniaxially aligned electrospun nanofibers, multi-channeled NGCs with variable channel numbers have also been reported.[36–38] However, the dimensions of the reported conduits were mostly restricted to an inner diameter of about 1.5 mm, which is not suitable for the repair of a thick nerve which contains several fascicles. For example, the effective diameter of a sciatic nerve in human can be as thick as 2–9 mm depending on the positions.[39] In another example, the effective diameter of the vastus medialis nerve is 5.0 ± 0.9 mm with an average of 7 ± 2 fascicles while that of the vastus lateralis nerve is 4.0 ± 1.0 mm with an average of 6 ± 2 fascicles.[40] Therefore, to repair a thick nerve, instead of simply using a large, single-tubular conduit, it is necessary to create multi-tubular NGC (mNGC) that is capable of dividing the space of a large lumen into multiple, smaller lumens to guarantee the guidance imposed by the conduit and mimic the fascicular structure of the nerve.

As one of the major cells in the native peripheral nerve, Schwann cells can be introduced prior to nerve regeneration so they are able to promote neurite growth by secreting neurotrophic molecules. A combination of scaffold and Schwann cells has shown marked improvement in the nerve regeneration and function recovery.[22,41–46] Due to the limited supply of autologous Schwann cells, bone marrow stem cells (BMSCs) have been transdifferentiated into Schwann cells and used as an alternative source to Schwann cells, leading to the enhancement of neurite outgrowth *in vitro*.[47–49] Compared with acellular conduits, cellular conduits have shown improvement in the repair of sciatic nerve injuries *in vivo*.[50,51] To our knowledge, there is no report on the transdifferentiation of BMSCs into Schwann cells in a nanofiber-based multi-tubular conduit with a diameter greater than 2 mm. With the incorporation of cellular component in a mNGC constructed from electrospun nanofibers with topographical cue, the regeneration of nerve should be further facilitated.

Herein, we report the fabrication of cellular, multi-tubular conduits with a honeycomb structure based on biodegradable electrospun nanofibers and cells derived from BMSCs. A bilayer mat of electrospun nanofibers is rolled up to form a single tube, with the inner and outer layers of the wall comprised of aligned and random fibers, respectively. Seven such tubes with an inner diameter of about 1.3 mm are then assembled into a hexagonal array and

encased within the lumen of a larger tube to obtain a multi-tubular conduit with an inner diameter of about 5.0 mm. The dimension of the conduit can be easily adjusted by tuning the size of the mat used for fabricating the small tubes. As a proof of concept, we have fabricated conduits with lengths of 2.2, 4.2, and 7.2 cm, respectively. In each conduit, seven channels can be aligned such to have six of them located peripherally and the other one in the center.[31,33] The conduit with a honeycomb structure mimics the anatomy of a native peripheral nerve. After characterization of the conduit, BMSCs are seeded into the conduit to examine the cell proliferation and distribution. The BMSCs can proliferate in all the tubes with even distributions along both longitudinal and circumferential directions and be further transdifferentiated into Schwann-like cells to obtain a cellular conduit that is promising for nerve tissue engineering.

2 Experimental Section

2.1 Chemicals and Materials

Dichloromethane (DCM), N,N-dimethylformamide (DMF), PCL (Mn≈80,000 g/mol), 0.1% poly-L-lysine solution, forskolin, and Cell Counting Kit-8 (CCK-8) were all purchased from Sigma-Aldrich. Laminin was obtained from Millipore. Bovine pituitary extract was obtained from Biomedical Tech Inc.. All other chemicals were ordered from Thermo Fisher Scientific. The water used in all experiments was obtained by filtering through a set of Millipore cartridges (Epure, Dubuque, IA).

2.2 Fabrication and Characterization of Electrospun Fibers

The fibers were fabricated using the traditional electrospinning process. PCL solution at a concentration of 12 wt.% was prepared by dissolving PCL in a mixture of DCM and DMF at a ratio of 6:4 (v/v). The polymer solution was ejected at a flow rate of 1.0 mL/h through a syringe pump. A high voltage (DC) of 12 kV was applied between the nozzle (a 22-gauge needle) and a rotating drum which was used as the grounded collector. A bilayer mat of electrospun fibers was fabricated by collecting the uniaxially aligned fibers for 2 h at a rotating speed of 500 rpm followed by collecting the random fibers for another 2 h at a rotating speed of 100 rpm. The morphologies of the aligned and the random fibers in the bilayer mat were characterized under a scanning electron microscope (SU8230). The average diameters of the fibers were measured using ImageJ software from 200 fibers in the scanning electron microscopy (SEM) images. Fast Fourier transform (FFT) analysis of the SEM images was also performed by utilizing the FFT function of the ImageJ software.

2.3 Fabrication of Multi-tubular Conduits

The bilayer mat was peeled off from the aluminum foil and the side composed of aligned fibers was treated with oxygen plasma for 2 min and sterilized under UV for 1 h. Then, small single tube was fabricated by rolling up this bilayer mat with the random fibers on the outer surface together with an inner surface of aligned fibers. The boundary of the tube was sealed using the same PCL solution. Afterwards, seven such small tubes were assembled into a hexagonal array and wrapped within the lumen of a larger tube. The interfaces among the small tubes, as well as between the small tubes and the large tube, were also fused using the PCL solution.

2.4 Characterization of the Multi-tubular Conduits

The morphology of the multi-tubular conduits was characterized using SEM. The conduits were frozen-embedded with the optimum cutting temperature (OCT) compound and then separately sectioned along the transversal and longitudinal-axis with a sectioning thickness of 80 μm using cryostat (CryoStar NX70). The sections were transferred onto a SEM specimen holder using double-sided adhesive tape and observed under the scanning electron microscope. The sections obtained by cutting the tube along the transversal axis were stained with fluorescein-conjugated bovine serum albumin (FITC-BSA) and imaged under a Leica 6000 B inverted microscope (Buffalo Grove, IL).

2.5 Growth of BMSCs in the Multi-tubular Conduits

We separately fabricated multi-tubular conduits with a length of 2.2, 4.2, and 7.2 cm by varying the dimensions of the mats. The conduits were then immersed in a 0.1% poly-L-lysine solution for 1 h at room temperature and then in a 50 μg/mL laminin solution at 4 °C overnight. BMSCs at passage 2, isolated from Lewis rat,[47] were seeded into the seven small tubes and the inner space among the large tube and small tubes at a density of 5×10^4 cells/cm^2. The conduits with a length of 2.2 cm were then incubated in the wells of a 6-well plate while the conduits with a length of 4.2 and 7.2 cm were incubated in cell culture tubes, and the conduits were continuously rotated for 2 h.

To demonstrate the survival of the cells in the conduits with incubation, the cells were incubated for 7 days with fresh medium replaced every 2 days and the cells' viabilities were detected at the time of incubating the cells for 1 day, 4 days, and 7 days by CCK-8 assay. The cells were washed with phosphate buffered saline (PBS) and then incubated in cell culture medium supplemented with CCK-8 reagent (10%). After 4 h, the absorbance value of the supernatant at 450 nm was measured using a microplate reader. The viability of the cells after incubation for 1 day was taken as 100%, and the viabilities of the cells after incubation for 4 and 7 days were calculated by comparing the corresponding absorbance of the supernatant to that after incubation for 1 day, respectively. The survival of cells in the conduits with different lengths were examined. Triplicate samples were used in each group.

To examine the morphology of the cells in the conduit, after incubation for 7 days, the cells were fixed in 3% glutaraldehyde solution at room temperature for 10 min. Then, the seven small tubes were cut open and adhered onto glass slides. The cells were permeabilized with 0.1% Triton X-100 for 5 min, blocked with 3% BSA for 1 h, and then incubated with Alexa Fluor 555 phalloidin for 20 min and 4', 6-Diamidine-2'-phenylindole dihydrochloride (DAPI) for 5 min, respectively. Fluorescence micrographs of cells in each tube were captured at different positions. The numbers of cells at different positions were counted using ImageJ software. The orientation of cells was evaluated by analyzing the two-dimensional FFT pattern and the angle deviation of cells from the corresponding fluorescence micrograph using ImageJ software.

2.6 Distribution of BMSCs in the Multi-tubular Conduits

The distribution of BMSCs in the conduit with a length of 4.2 cm was examined along both the longitudinal and axial directions. After incubating the BMSCs in the conduit for 7 days,

we fixed the cells and frozen-embedded the conduit with OCT compound and then sectioned the conduit along a direction either perpendicular or parallel to the longitudinal-axis of the conduit using cryostat at a sectioning thickness of 10 μm. When cutting the conduit along the direction perpendicular to the longitudinal axis, we collected sections at the midpoint and the two ends of the conduit. When cutting the conduit parallel to the longitudinal axis, we collected sections at the central and boundary positions of the conduit. At least ten sections were collected within each region. The sections were mounted onto glass slides and then stained with Alexa Fluor 555 phalloidin and DAPI to reveal the F-actins and cell nuclei, respectively. Fluorescence micrographs were captured using a laser confocal scanning microscope (Zeiss LSM 700) with a tile scanning approach. Triplicate samples were used in each group.

2.7 Differentiation of BMSCs in the Multi-tubular Conduits

The BMSCs were induced into Schwann cell-like phenotypes in the conduits under chemical treatment according to our previous protocol.[47] Briefly, at 24 h post seeding, the cells were treated with culture medium supplemented with 1 μM β-mercaptoethanol for 24 h, 35 ng/mL all-trans-retinoic acid for 72 h, and then growth factor cocktails (5 ng/mL platelet derived growth factor-AA, 10 ng/mL basic fibroblast growth factor, 126 ng/mL glial cell-derived growth factor, and 5.7 μg/mL forskolin) for another 2 weeks with fresh medium replaced every 3 days, respectively.

2.8 Characterization of the Derived Cells in the Multi-tubular Conduits

After the transdifferentiation in the conduit, the cells were fixed, and then the seven small tubes were cut open and adhered onto glass slides. The cells were stained with Alexa Fluor 555 phalloidin and DAPI using the same procedures as described above. Fluorescence imaging was performed using the fluorescent microscope. The numbers of cells at different positions were counted using ImageJ software. The orientation of cells was evaluated by analyzing the two-dimensional FFT pattern and the angle deviation of cells from the corresponding fluorescence micrograph using ImageJ software.

We also performed immunofluorescence staining to monitor phenotypic changes to BMSCs using S100 as a general indicator for Schwann cells. The cells were fixed in 3% glutaraldehyde solution at room temperature for 10 min, permeabilized with 0.1% Triton X-100 for 5 min, blocked with 3% BSA and 5% goat serum for 1 h, and then incubated with rabbit anti-S100 antibody overnight at 4 °C. The anti-S100 marker was detected using Alexa Fluor 488 goat anti-rabbit IgG (1:200) secondary antibody, followed by DAPI staining for cell nuclei. In a control group, the undifferentiated BMSCs cultured on tissue culture plate were stained with Alexa Fluor 555 phalloidin, anti-S100, and DAPI. Immunofluorescence micrographs were captured using the fluorescent microscope. The fluorescence intensities of the cells at different positions were evaluated by measuring the mean pixel intensities of the micrographs using ImageJ software (n=3). We also stained the derived cells that were located in the midpoint of the central, small tube of the conduit with S100 and CD44 antibodies. The cells were incubated with primary antibodies (rabbit anti-S100 and mouse anti-CD44) and then with secondary antibodies (Alexa Fluor 555 goat-anti-rabbit IgG and

Alexa Fluor 488 goat-anti-mouse IgG). As a control, the undifferentiated BMSCs cultured on tissue culture plate were stained with Alexa Fluor 555 phalloidin, anti-CD44, and DAPI.

We also quantified the mRNA expression levels of representative genes expressed by the derived cells in the small tubes at different locations using real time polymerase chain reaction (PCR) analysis. After transdifferentiation, the seven small tubes were separated off from the large tube using a blade, and then the expressions of the genes in the derived cells of each tube were separately examined using the same method as we reported previously.[47] In a control group, the cells were transdifferentiated on the bilayer mat used for construct the conduit, and the expressions of genes in the derived cells were examined. Four genes were evaluated in our study: BMPR1a (bone morphogenetic protein receptor, type IA), CD44, S100, and p75 along with the housekeeping gene glyceraldehyde phosphate dehydrogenase (GAPDH). The gene expression was normalized to GAPDH in the same sample. The primers we used were listed in Table S1.

We then investigated the survival of the derived cells in the conduit as following. The differentiation medium was switched to the Schwann cell medium which contained Dulbecco's modified Eagle medium (DMEM) supplemented with 10% fetal bovine serum (FBS), 1% antibiotic-antimycotic, 2 μM forskolin and 20 μg/mL bovine pituitary extract. The cells were then incubated for 7 days with fresh medium replaced every 2 days. The viabilities of the cells after incubation for 1 day, 3 days, 5 days, and 7 days were analyzed, respectively, by CCK-8 assay. We also investigated the function of the derived cells by analyzing the secreted protein level. After the derived cells had been incubated in the Schwann cell medium for 7 days, the secreted nerve growth factor (NGF) content in the medium was detected using NGF Elisa kit according to the manufacturer's instructions. The cells were then fixed and stained with anti-S100 using the same procedures as described above.

2.9 Distribution of the Derived Cells in the Multi-tubular Conduits

The distributions of the derived cells in the conduit along both the transversal and longitudinal axes were further characterized. After transdifferentiation, the derived cells in the conduit were fixed. Then, we frozen-embedded the conduit with OCT compound and then sectioned the conduit along a direction either perpendicular or parallel to the longitudinal-axis using cryostat at a sectioning thickness of 10 μm. The sections at different positions of the conduit were collected and mounted onto glass slides. The cells on the collected sections were then immuno-stained with Alexa Fluor 488 anti-S100. The F-actins and cell nuclei were stained with Alexa Fluor 555 phalloidin and DAPI, respectively. Fluorescence micrographs were captured using a laser confocal scanning microscope with a tile scanning approach. Triplicate samples were used in each group.

2.10 Statistical Analysis

Each experiment was repeated for three times and all datasets were expressed in terms of mean and standard deviations. Statistical analysis was performed using the Student's t test in SPSS. Differences were considered statistically significant when $P < 0.05$.

3 Results and Discussion

3.1 Structure and Morphology of the Multi-tubular Conduits

We fabricated a bilayer mat made of electrospun PCL fibers with one layer containing uniaxially aligned fibers and the other layer random fibers by controlling the rotating speed of the drum. PCL was used to fabricate the nanofibers because PCL is a hydrophobic, semi-crystalline polymer with good biocompatibility and biodegradability. The degradation of PCL is a two-stage process. In the first stage, the PCL undergoes random hydrolytic chain scission of the ester linkages, resulting in a decrease in molecular weight. Once the polymer is less than 3000 in low molecular weight, it undergoes intracellular degradation. The scaffold made of PCL can be completely resorbed and degraded within about 1–4 years *in vivo*.[52–55] Figure S1A shows SEM image of a typical sample made of uniaxially aligned fibers with an average diameter of 971 ± 42 nm. FFT pattern of the image confirms that the fibers were uniaxially aligned as the pixel intensities showed dependence on the direction. Figure S1B shows SEM image of the random fibers with an average diameter of 1018 ± 53 nm. The random orientation was further confirmed by the corresponding FFT pattern.

We then fabricated a small tube by rolling up this bilayer mat with the random fibers on the outer surface to circumvent any possible tearing during surgery, together with an inner layer of uniaxially aligned fibers to provide longitudinal guidance for axon extension (Figure 1, A and B).[22,23,56] The boundary of the tube was then sealed using the PCL solution that was used for electrospinning. Afterwards, we assembled seven such small tubes into a hexagonal array and wrapped inside the lumen of a larger tube, as the cross-section illustrated in Figure 1C. One small tube was located at the center while the other were located in the periphery. The resultant honeycomb structure mimics the anatomy of a peripheral nerve.[57] Besides, the lumen diameters and lengths of both the small and large tubes can be easily tuned according to the actual fascicle numbers and size of the nerve to be repaired. Figure 1D shows a photograph taken from the cross section of a multi-tubular conduit, revealing the honeycomb structure. When the conduit was stained with FITC-BSA, as shown in the inserted fluorescence micrograph in Figure 1D, the honeycomb structure can be clearly observed. In a typical sample, seven small tubes with an inner diameter of about 1.3 mm were assembled and then wrapped in a larger tube to form a conduit with an inner diameter of about 5.0 mm. Conduits with a length of 2.2, 4.2, and 7.2 cm were separately fabricated. To guarantee the rigidity of the structure, we fused the interfaces among the small tubes, as well as between the small tubes and the large tube, using the PCL solution. The conduits could keep their shapes without being broken when soaked in water, PBS, and cell culture medium. After soaked in PBS for three months, the conduits preserved the honeycomb structure without collapsing. In a pilot study, the conduits were also demonstrated to be strong enough to resist the handling and tearing during suturing.

We then characterized the structure and morphology of the conduits using SEM. From Figure 2, A and B, at a low magnification, we can resolve the overall morphology of the cross-section of the conduit to confirm a honeycomb structure. As shown in Figure 2C, most of the fibers point out away from the image, indicating the uniaxial alignment of the fibers within the inner side of the small tube. From the longitudinal view of the mNGC (Figure 2,

D-E), the wall of the small tubes can be clearly observed with the highly porous structures preserved. As shown in Figure 2F, most of the fibers point toward random directions.

3.2 Growth of BMSCs in the Multi-tubular Conduits

We then examined the growth of BMSCs in the conduit. To improve nerve repair, the cellular mNGC should contain Schwann cells at the highest possible density. From our previous study,[47] laminin-coated fibers with a diameter of about 1.0 μm showed the best performance in inducing the differentiation of BMSCs into Schwann-like cells. In this study, we controlled the average diameter of the fibers at about 1.0 μm and coated their surfaces with laminin. After incubating the BMSCs for 7 days, we observed the morphologies of the cells at different positions, including the midpoint and the two ends, in each tube. Here we only show the representative morphological images of cells in the small tubes of a conduit with a length of 4.2 cm. Figure 3A shows the representative fluorescence micrograph of the cells at the midpoint of the small tube that was located at the center of the conduit. The BMSCs adhered to and grew healthily on the electrospun fibers and almost covered the entire surface of the tube at a high confluency. Besides, the BMSCs showed an actin network consisting of a large number of filaments aligned parallel to the long axes of the underlying fibers, indicating the contact guidance of the fibers to the BMSCs. The fluorescence micrographs of the cells at the midpoints of two small tubes that were located at opposite sites in the periphery of the conduit are shown in Figure 3, B and C. The cells showed similar morphologies to those in Figure 3A, indicating that the small tubes supported the growth of BMSCs regardless of the locations in the conduit. The representative micrographs of the cells located at two ends of the small tubes are shown in Figure S2. At different positions in each tube, either at the two ends or in the middle region, the cells showed similar morphologies.

We further analyzed the numbers of cells at different positions of the conduit. Based on Figure S3, there were no significant differences in the densities of cells among different positions, indicating that BMSCs were distributed evenly over the inner surfaces of the tubes. The orientations of cells that were located in the middle regions of the small tubes were further quantified by FFT analysis of the corresponding fluorescence micrographs. As shown in Figure S4, regardless of the positions of the cells, FFT patterns of the micrographs confirm that the orientations of the cell's filaments showed dependence on direction. In the middle region of the small tube that was located at the center of the conduit (Figure S4A), 82% of cells were aligned within an angle deviation of 20 degree, indicating the highly-oriented architecture of the cells. From Figure S4, B and C, the cells in the two small tubes that were located at the opposite sites in the periphery of the conduit also showed high degree of orientation.

To investigate the biocompatibility of the conduit as well as the survival of BMSCs in the conduit, we separately examined the viabilities of cells in the conduits with different lengths using CCK-8 assay after incubation for different periods of time. The viability of the cells after incubation for 1 day was taken as 100%. As shown in Figure 3D, in a conduit with a length of 2.2 cm, the viability of cells increased with incubation time ($P<0.05$, $n=3$), indicating that the cells were alive and proliferative in the conduit. Even in a long conduit

with a length of 7.2 cm, after incubation for 7 days, the viability of the cells was higher than that at 1 day ($P<0.05$, $n=3$). The highly porous structure intrinsic to a mat of electrospun fibers ensures adequate transportation of nutrients and wastes between cells and surroundings to keep the cells alive.

3.3 Distribution of BMSCs in the Multi-tubular Conduits

We further examined the distribution of BMSCs in the conduit after incubation for 7 days along both the longitudinal and axial directions by taking the 4.2 cm conduit as an example. The representative fluorescence micrographs of the BMSCs in the conduit are shown in Figure 4. From Figure 4, A-C, we can observe the circumferential distribution of cells in each small tube. Along the longitudinal axis of the conduit, the circumferential distribution of the cells showed no major differences with the positions, indicating that the cells kept alive over the longitudinal axis of all the seven small tubes. Figure 4, D and E, show the cells distribution at the central and boundary area of the conduit, respectively. The inserted image shows an overlay of the fluorescence micrograph and the bright-field image to indicate the locations of cells in the conduit. From Figure 4D, along the longitudinal axis of the conduit, the cells almost covered on the entire surface. Among different small tubes, the distribution of cells showed no major differences. Especially, in the small tube that was located at the center of the conduit, we still found the presence of cells. Similar distribution of cells was also found in Figure 4E for the boundary area of the conduit, indicating that the cells were distributed evenly not only along but also perpendicular to the longitudinal axis of the conduit. This can be attributed to the well-controlled cell seeding procedure and the continuous rotation of the conduit during the incubation, which ensured the adhesion of BMSCs in all the small tubes. The even distribution of BMSCs in all the small tubes is of great importance for ensuring the uniform distribution of derived cells in the whole conduit for guiding axon regeneration.

3.4 Transdifferentiation of BMSCs in the Multi-tubular Conduits

We further induced the transdifferentiation of BMSCs into Schwann cells in the conduit. From the F-actin staining of the derived cells at different positions in the conduit as shown in Figure S5, after transdifferentiation, the cells demonstrated a bipolar and spindle shape that resembled the typical morphology of Schwann cells.[22] Regardless of the positions, either at the midpoint or the two ends of the small tubes that were located at the center or in the periphery of the conduit, the cells covered most part of the surfaces. From the statistical analysis of the cell densities, as shown in Figure S6, no significant differences were found among the different positions. The orientations of the derived cells were further quantified through FFT analysis of the corresponding fluorescence micrographs. As shown in Figure S7A, in the midpoint of the small tube that was located in the center of the conduit, the orientation of the cells' filaments showed dependence on direction. Similar patterns were also found for the cells in the two small tubes that were located at opposite sites in the periphery of the conduit (Figure S7, B and C). The derived cells responded to the topographical cues presented by the underlying fibers and showed an aligned actin network.

We performed immunofluorescence staining to evaluate the transdifferentiation efficiency of the BMSCs by examining the expression of protein S100, which is a specific marker of

Schwann cells, in the derived cells. In the control group, as shown in Figure S8, no expression of S100 was found in the undifferentiated BMSCs cultured on a tissue culture plate. After transdifferentiation in the conduit, the representative fluorescence micrographs of the derived cells located at the midpoints of the small tubes were shown in Figure 5, A-C. From the micrographs, the derived cells all expressed S100 regardless of the location of the small tubes. From the statistical analysis of the fluorescence intensities of the cells at different positions (Figure 5D), no significant differences were found among different small tubes (n=3). We also stained the derived cells in the midpoint of the small tube that was located at the center of the conduit with S100 and CD44 antibodies. In the control group, all undifferentiated BMSCs expressed CD44, as shown in Figure S9. After transdifferentiation, from the representative immunofluorescence micrographs in Figure S10, a small portion of cells were found to co-express S100 and CD44. Quantitative analysis showed that the percentage of cells that co-expressed S100 and CD44 was 16.3 ± 5.4% (n=3), which could be attributed to either the derived cells or a small portion of undifferentiated BMSCs. Therefore, to be precise, the derived cells are referred as Schwann-like cells. We can conclude that the expression of CD44 in the cells were significantly decreased after transdifferentiation.

We also quantified the mRNA expression levels of representative genes expressed by the derived cells in the small tubes at different locations. The expression of the genes related to BMSCs (BMPR1a and CD44) and the genes related to Schwann cells (S100 and p75) in the derived cells were analyzed. We have confirmed that BMSCs could be transdifferentiated into Schwann-like cells on the mat of laminin-coated, uniaxially aligned electrospun fibers in high efficiency (Figure S11).[47] Here, we further compared the relative transcript levels expressed in the derived cells that were transdifferentiated in the conduit with that on a bilayer mat containing the typically same uniaxially aligned fibers. The relative transcript level of genes expressed in the cells transdifferentiated on the mat was taken as the control and set as 1.0 to calculate the fold of relative transcript level of the corresponding genes expressed in the cells transdifferentiated in the conduit. From Figure 6A, compared with the cells differentiated on the mat, the expression levels of BMSC-related genes in the cells differentiated in the conduit showed no statistical major differences. In the conduit, the expressions of Schwann cell-related genes also showed no significant differences when compared with that on the mat of electrospun fibers. Therefore, the BMSCs could be transdifferentiated into Schwann-like cells in the conduit in high efficiency.

It is important to ensure that the derived cells could survive either for the purpose of transportation or for remaining viable after transplantation into the body. We further incubated the derived cells in the conduit in the Schwann cell medium for 7 days. During the incubation, the cell viabilities were analyzed using CCK-8 assay. As shown in Figure 6B, the cells remained alive and even proliferated over time. After incubation for 7 days, the viability of the cells was significantly higher than that at 1 day ($P<0.05$, n=3). We also evaluated the secretion of NGF from the derived cells using NGF Elisa after incubation for 7 days. The derived cells in the conduit were capable of secreting NGF at an amount of 509 ± 58 pg (n=3). Figure S12 shows the representative immunofluorescence micrograph of the derived cells in the midpoint of the small tube that was located at the center of the conduit after incubation in the Schwann cell medium for 7 days. All the cells expressed S100,

indicating that the derived cells retained the differentiated state which could be attributed to the high degree of differentiation of BMSCs in the conduit. Taken together, these results demonstrated that the BMSCs could be induced to effectively transdifferentiate into Schwann-like cells in the multi-tubular conduit and the derived cells could survive and secret NGF with the transdifferentiated state retained.

3.5 Distribution of the Derived Cells in the Multi-tubular Conduits

We further evaluated the distribution of the derived Schwann-like cells in the conduit. Similar to the scrutiny of BMSCs in the conduit as described above, we analyzed the distribution of the derived cells at different positions along both the transversal and longitudinal axes of the conduit. The representative fluorescence micrographs of the derived cells in the conduit are shown in Figure 7. From the cross-sectional view, in all the seven small tubes, the derived cells were presented and distributed over the circumferential direction of the tube (Figure 7, A-C). Besides, at different positions of the conduit along the longitudinal axis, the presence of cells in each small tube showed no major differences, indicating that the derived cells kept alive over the longitudinal axis of the small tube. Figure 7, D and E, show the distribution of the derived cells at the center and boundary area of the multi-tubular conduit, respectively. It is clear that the cells were presented in the small tubes that were located either at the center or in the periphery of the conduit. Among the different small tubes, the cells densities showed some differences. Since the cells did not cover the entire surface of the tube, there would be some regions that were not occupied by cells in the section. Besides, because of the angle deviation of the cells orientation, when we cut the conduit along the longitudinal axis of the conduit, we may obtain the cross-sections of some cell bodies, resulting in those dots in the image. From these results, we can conclude that the BMSCs could be transdifferentiated into Schwann-like cells in the conduit and the derived cells were distributed over the conduit. The seven small tubes and the derived cells in them would be beneficial to guiding and promoting the axon regrowth to improve the repair of long lesions in thick nerves.

4 Conclusions

In summary, we have demonstrated the fabrication of multi-tubular conduits with a honeycomb structure based on electrospun nanofibers by mimicking the native fascicular structure of a peripheral nerve. Seven small tubes were assembled into a hexagonal array and wrapped within the lumen of a larger tube to obtain the multi-tubular conduit. Both the diameter and length of the conduit could be easily tailored to match the actual size of the target nerve to be repaired. The fabricated conduit was robust enough for handling and tearing during surgery. The seeded BMSCs were able to proliferate in all the small tubes with even distributions along both the circumferential and longitudinal directions. Under chemical induction, the BMSCs were transdifferentiated into Schwann-like cells in the conduit. The cellular conduit holds great promise for the repair of long lesions in thick nerves. The multi-tubular conduits can be further improved by combing with growth factors to enhance nerve regeneration and applied in nerve tissue engineering. In addition, this multi-tubular structure can be employed to investigate the fundamental aspects involved in the development of peripheral nervous system and migration of cells.

Supplementary Material

Refer to Web version on PubMed Central for supplementary material.

Acknowledgements

This work was supported in part by a grant from the National Institutes of Health (R01 EB020050) and startup funds from the Georgia Institute of Technology.

References

[1]. Scheib J, Höke A, Nat. Rev. Neurol 2013, 9, 668. [PubMed: 24217518]

[2]. de Villiers Alant JD, Senjaya F, Ivanovic A, Forden J, Shakhbazau A, Midha R, PloS One 2013, 8, e82546. [PubMed: 24282624]

[3]. Rochkind S, Shapira Y, Nevo Z, Future Neurol 2014, 9, 105.

[4]. Bellamkonda RV, Biomaterials 2006, 27, 3515. [PubMed: 16533522]

[5]. Hudson TW, Evans GR, Schmidt CE, Orthop. Clini 2000, 31, 485.

[6]. Gu X, Ding F, Yang Y, Liu J, Prog. Neurobiol 2011, 93, 204. [PubMed: 21130136]

[7]. Marquardt LM, Sakiyama-Elbert SE, Curr. Opin. Biotechnol 2013, 24, 887. [PubMed: 23790730]

[8]. Nectow AR, Marra KG, Kaplan DL, Tissue Eng., Part B 2011, 18, 40.

[9]. Pabari A, Yang SY, Mosahebi A, Seifalian AM, J. Controlled Release 2011, 156, 2.

[10]. Pabari A, Yang SY, Seifalian AM, Mosahebi A, J. Plast. Reconstr. Aesthet. Surg 2010, 63, 1941. [PubMed: 20061198]

[11]. Kehoe S, Zhang X, Boyd D, Injury 2012, 43, 553. [PubMed: 21269624]

[12]. Chiono V, Tonda-Turo C, Prog. Neurobiol 2015, 131, 87. [PubMed: 26093353]

[13]. Xue C, Zhu H, Tan D, Ren H, Gu X, Zhao Y, Zhang P, Sun Z, Yang Y, Gu J, Gu Y, Gu X, J. Tissue Eng. Regener. Med 2018, 12, e1143.

[14]. Amy MM, Rahul K, Christina KM, Farhadi HF, Gregory HB, Susan EM, Hand 2009, 4, 180. [PubMed: 19137378]

[15]. Saracino GAA, Cigognini D, Silva D, Caprini A, Gelain F, Chem. Soc. Rev 2013, 42, 225. [PubMed: 22990473]

[16]. Abidian MR, Daneshvar ED, Egeland BM, Kipke DR, Cederna PS, Urbanchek MG, Adv. Healthcare Mater 2012, 1, 762.

[17]. Hu Y, Wu Y, Gou Z, Tao J, Zhang J, Liu Q, Kang T, Jiang S, Huang S, He J, Chen S, Du Y, Gou M, Sci. Rep 2016, 6, 32184. [PubMed: 27572698]

[18]. Li D, Wang Y, Xia Y, Nano Lett 2003, 3, 1167.

[19]. Li D, Wang Y, Xia Y, Adv. Mater 2004, 16, 361.

[20]. Xie J, Li X, Xia Y, Macromol. Rapid Commun 2008, 29, 1775. [PubMed: 20011452]

[21]. Xie J, Liu W, MacEwan MR, Bridgman PC, Xia Y, ACS Nano 2014, 8, 1878. [PubMed: 24444076]

[22]. Xie J, MacEwan MR, Liu W, Jesuraj N, Li X, Hunter D, Xia Y, ACS Appl. Mater. Interfaces 2014, 6, 9472. [PubMed: 24806389]

[23]. Xie J, MacEwan MR, Schwartz AG, Xia Y, Nanoscale 2010, 2, 35. [PubMed: 20648362]

[24]. Cao H, Liu T, Chew SY, Adv. Drug Delivery Rev 2009, 61, 1055.

[25]. Kim Y, Haftel VK, Kumar S, Bellamkonda RV, Biomaterials 2008, 29, 3117. [PubMed: 18448163]

[26]. Madduri S, Papaloizos M, Gander B, Biomaterials 2010, 31, 2323. [PubMed: 20004018]

[27]. Liu W, Thomopoulos S, Xia Y, Adv. Healthcare Mater 2012, 1, 10.

[28]. Huang C, Ouyang Y, Niu H, He N, Ke Q, Jin X, Li D, Fang J, Liu W, Fan C, ACS Appl. Mater. Interfaces 2015, 7, 7189. [PubMed: 25786058]

[29]. Toba T, Nakamura T, Shimizu Y, Matsumoto K, Ohnishi K, Fukuda S, Yoshitani M, Ueda H, Hori Y, Endo K, J. Biomed. Mater. Res., Part A 2001, 58, 622. [PubMed: 11745513]

[30]. Yao L, de Ruiter GCW, Wang H, Knight AM, Spinner RJ, Yaszemski MJ, Windebank AJ, Pandit A, Biomaterials 2010, 31, 5789. [PubMed: 20430432]

[31]. de Ruiter GC, Onyeneho IA, Liang ET, Moore MJ, Knight AM, Malessy MJ, Spinner RJ, Lu L, Currier BL, Yaszemski MJ, Windebank AJ, J. Biomed. Mater. Res., Part A 2008, 84, 643.

[32]. Arcaute K, Mann BK, Wicker RB, Tissue Eng., Part C 2011, 17, 27.

[33]. Sun C, Jin X, Holzwarth JM, Liu X, Hu J, Gupte MJ, Zhao Y, Ma PX, Macromol. Biosci 2012, 12, 761. [PubMed: 22508530]

[34]. Liu S, Sun X, Wang T, Chen S, Zeng C, Xie G, Zhu Q, Liu X, Quan D, Mater. Sci. Eng., C 2018, 83, 130.

[35]. Scott JB, Afshari M, Kotek R, Saul JM, Biomaterials 2011, 32, 4830. [PubMed: 21492932]

[36]. Jeffries EM, Wang Y, Biotechnol. Bioeng 2012, 109, 1571. [PubMed: 22179932]

[37]. Jeffries EM, Wang Y, Biofabrication 2013, 5, 035015. [PubMed: 23945055]

[38]. Dinis TM, Elia R, Vidal G, Dermigny Q, Denoeud C, Kaplan DL, Egles C, Marin F, J. Mech. Behav. Biomed. Mater 2015, 41, 43. [PubMed: 25460402]

[39]. Grinberg Y, Joseph S, J. Rehabil. Res. Dev 2012, 49, 309. [PubMed: 22773531]

[40]. Gustafson KJ, Pinault GC, Neville JJ, Syed I, Davis JA, Jr, Jean-Claude J, Triolo RJ, J. Rehabil. Res. Dev 2009, 46, 973. [PubMed: 20104420]

[41]. Rodríguez FJ, Gómez N, Perego G, Navarro X, Biomaterials 1999, 20, 1489. [PubMed: 10458562]

[42]. Hadlock T, Sundback C, Hunter D, Cheney M, Vacanti JP, Tissue Eng 2000, 6, 119. [PubMed: 10941207]

[43]. di Summa PG, Kalbermatten DF, Pralong E, Raffoul W, Kingham PJ, Terenghi G, Neurosci 2011, 181, 278.

[44]. Daly W, Yao L, Zeugolis D, Windebank A, Pandit A, Soc JR, Interface 2012, 9, 202. [PubMed: 22090283]

[45]. Deumens R, Bozkurt A, Meek MF, Marcus MAE, Joosten EAJ, Weis J, Brook GA, Prog. Neurobiol 2010, 92, 245. [PubMed: 20950667]

[46]. Gu X, Ding F, Williams DF, Biomaterials 2014, 35, 6143. [PubMed: 24818883]

[47]. Xue J, Yang J, O'Connor DM, Zhu C, Huo D, Boulis NM, Xia Y, ACS Appl. Mater. Interfaces 2017, 9, 12299. [PubMed: 28322042]

[48]. Dezawa M, Takahashi I, Esaki M, Takano M, Sawada H, Eur. J. Neurosci 2001, 14, 1771. [PubMed: 11860471]

[49]. Sharma AD, Zbarska S, Petersen EM, Marti ME, Mallapragada SK, Sakaguchi DS, J. Biosci. Bioeng 2016, 121, 325. [PubMed: 26371993]

[50]. Ao Q, Fung C, Tsui AY, Cai S, Zuo H, Chan Y, K Shum D, Biomaterials 2011 32, 787. [PubMed: 20950852]

[51]. di Summa PG, Kingham PJ, Campisi CC, Raffoul W, Kalbermatten DF, Neurosci. Lett 2014 572, 26. [PubMed: 24792394]

[52]. Ali SAM, Zhong SP, Doherty PJ, Williams DF, Biomaterials 1993, 14, 648. [PubMed: 8399961]

[53]. Woodward SC, Brewer PS, Moatamed F, Schindler A, Pitt CG, J. Biomed. Mater. Res 2004, 19, 437.

[54]. Sun H, Mei L, Song C, Cui X, Wang P, Biomaterials 2006, 27, 1735. [PubMed: 16198413]

[55]. Woodruff MA, Hutmacher DW, Prog. Polym. Sci 2010, 35, 1217.

[56]. Xie J, MacEwan MR, Li X, Sakiyama-Elbert SE, Xia Y, ACS Nano 2009, 3, 1151. [PubMed: 19397333]

[57]. Flores AJ, Lavemia C, Owens PW, Am. J. Orthop 2000, 29, 167. [PubMed: 10746467]

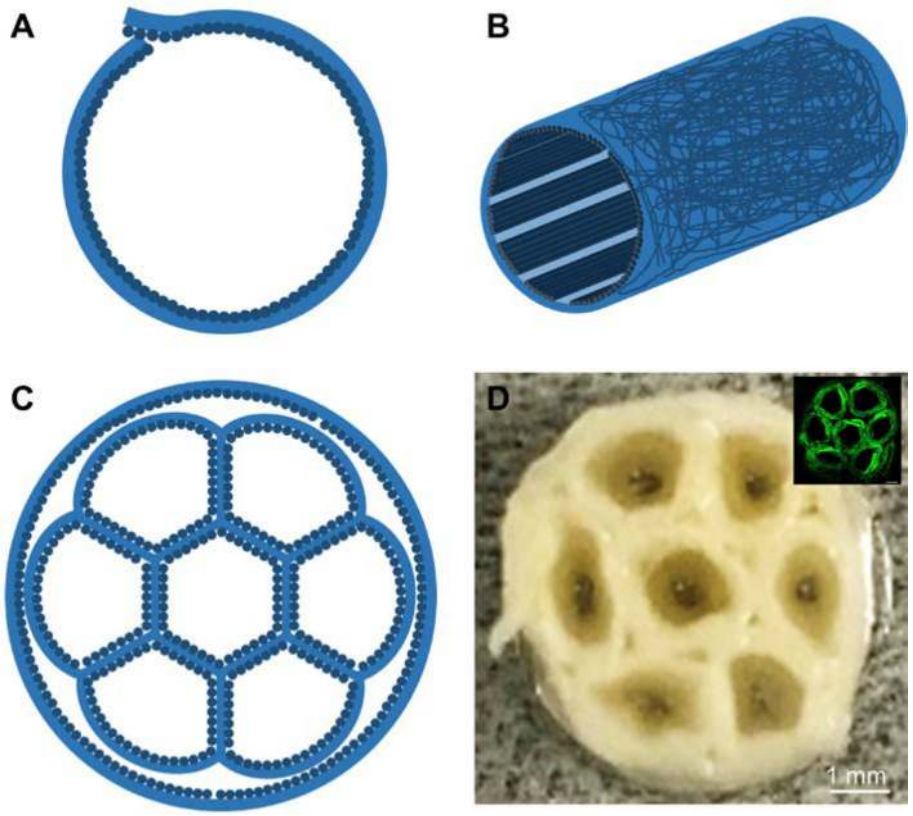

Figure 1.

Schematics showing (A) the cross-sectional and (B) side views of a single tube with a bilayer structure for the wall, which is comprised of random fibers as the outer layer and uniaxially aligned fibers as the inner layer, and (C) the cross-section of a multi-tubular conduit consisting of seven small tubes within the lumen of a large tube. (D) Photograph of the cross section of a multi-tubular conduit. The inset shows the fluorescence micrograph of the cross section of a conduit after the adsorption of FITC-BSA.

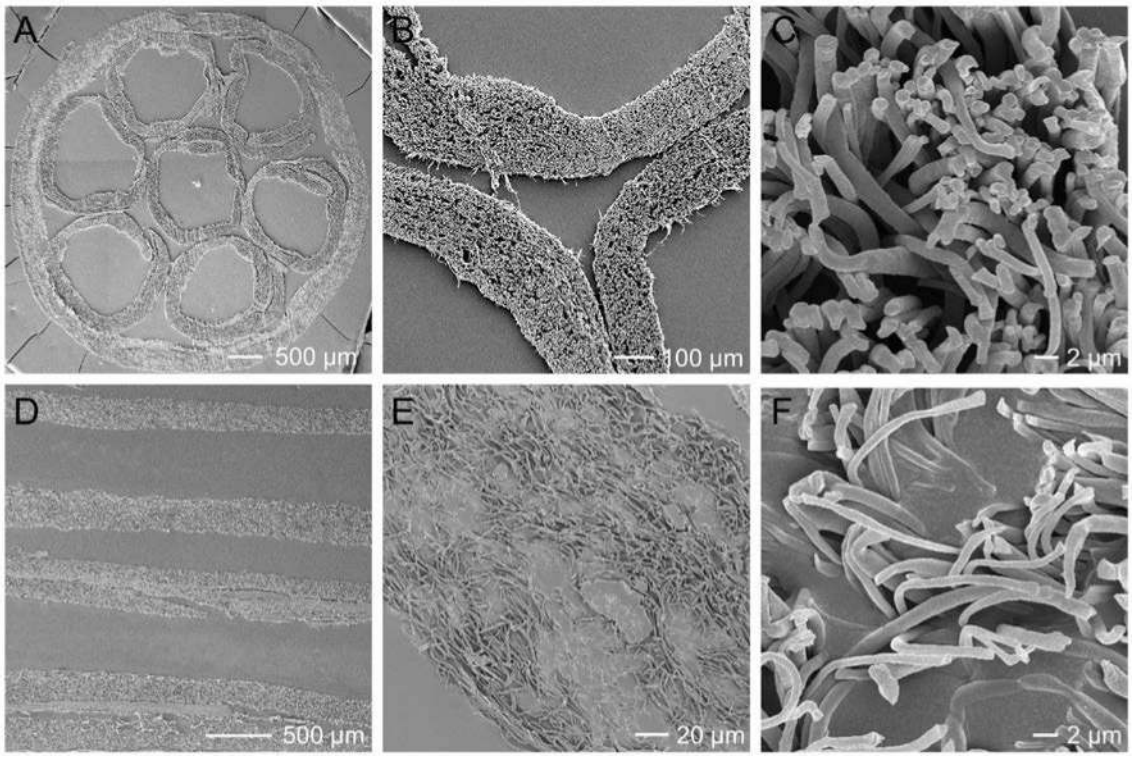

Figure 2.
SEM images of the multi-tubular conduit at different magnifications when the conduit was cryo-sectioned along (A-C) cross-sectional and (D-F) longitudinal directions, respectively.

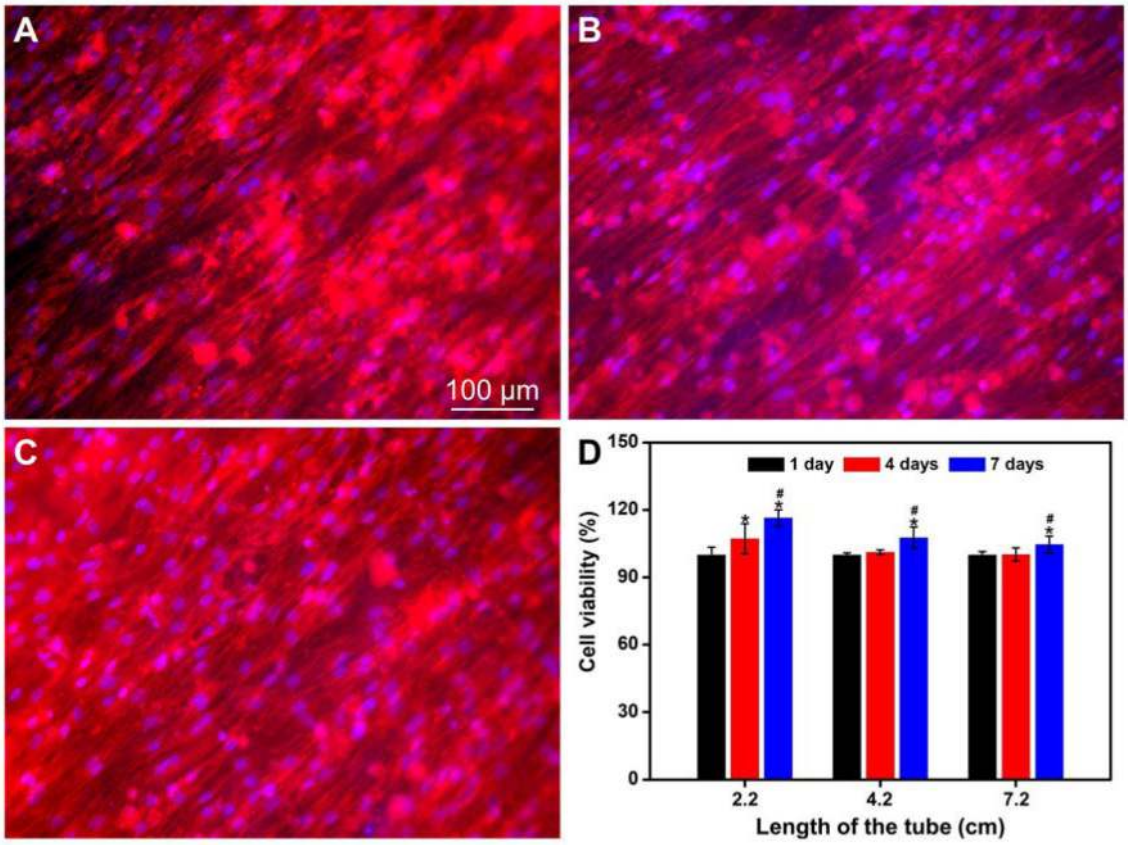

Figure 3.

Fluorescence micrographs of the BMSCs after incubation in the multi-tubular conduit (length = 4.2 cm) for 7 days. The small tubes were cut open and then the F-actins of the cells were stained with Alexa Fluor 555 phalloidin (red) while the cell nuclei were stained with DAPI (blue). The images were captured from the middle region of the small tubes, which were located (A) at the center and (B, C) in the periphery at opposite sites of the conduit, respectively. (D) Viabilities of BMSCs after incubation in the conduit with lengths of 2.2, 4.2, and 7.2 cm for different periods of time. *$P < 0.05$ compared with that at 1 day ($n = 3$). $^{\#}P < 0.05$ compared with that at 4 days ($n = 3$).

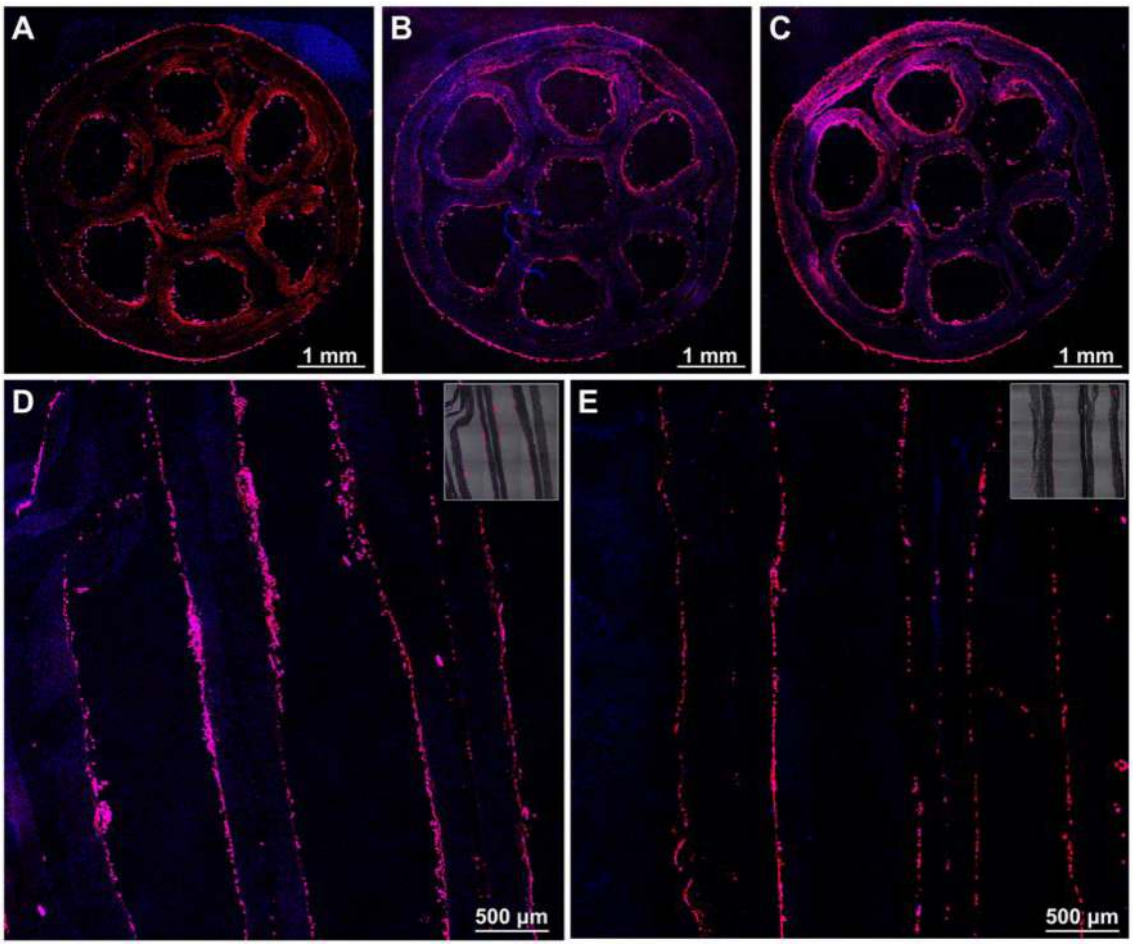

Figure 4.

Fluorescence micrographs of the BMSCs distributed in the multi-tubular conduit with a length of 4.2 cm after incubation for 7 days. The conduit was frozen sectioned along the direction perpendicular to the longitudinal axis at the (A) proximal, (B) center, and (C) distal positions, and along direction parallel to the longitudinal axis at the (D) center and (E) boundary areas, respectively. F-actins of the cells were stained with Alexa Fluor 555 phalloidin (red) while the cell nuclei were stained with DAPI (blue). The inserted images at the top right corners in (D) and (E) are the overlay of fluorescence micrograph and the corresponding bright-field image.

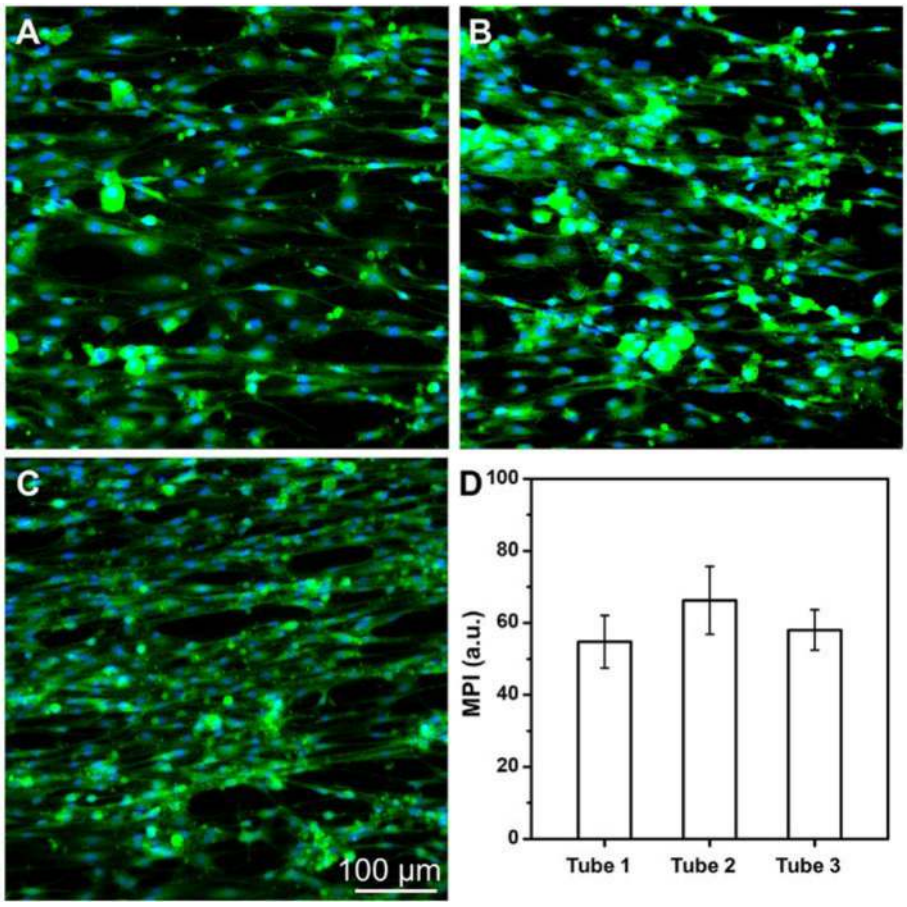

Figure 5.

Representative fluorescence micrographs of the derived cells in the middle regions of the small tubes that were located (A) at the center (tube 1) and (B, C) in the periphery at opposite sites (tube 2 and tube 3) of the multi-tubular conduit, respectively, after transdifferentiation in the conduit with a length of 4.2 cm. The small tubes were cut open, and then the S100 protein were stained with Alexa Fluor 488 anti-S100 (green) and the cell nuclei were stained with DAPI (blue), respectively. (D) Mean pixel intensity (MPI) analysis of S100 expression from the derived cells in the middle regions of the different small tubes. No significant differences of the MPI were found among different tubes (n = 3).

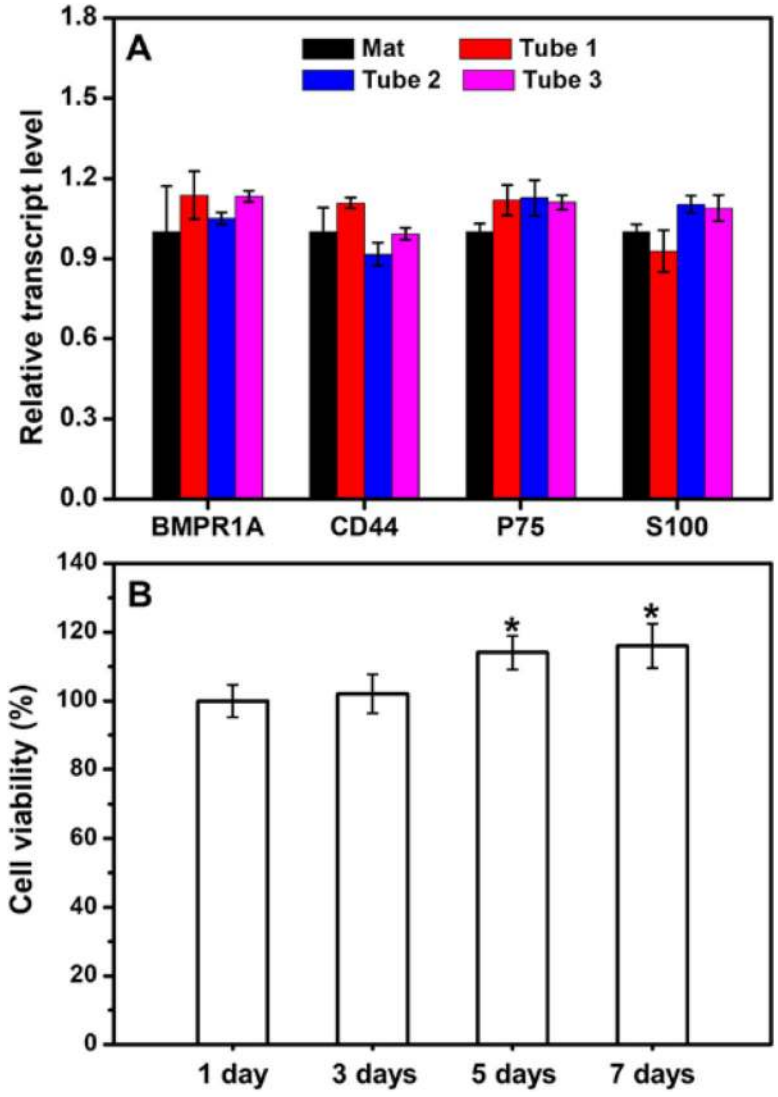

Figure 6.

(A) Real-time PCR analysis showing the relative transcript levels of the genes related to BMSCs and Schwann cells expressed in the derived cells differentiated in the conduit and on a bilayer mat consisted of laminin-coated uniaxially aligned fibers. Tube 1 represents the small tube that was located at the center of the conduit while tube 2 and tube 3 represent the two small tubes that were located in the periphery of the conduit at opposite sites. (B) Viabilities of the derived cells in the conduit after incubation for different periods of time in the Schwann cell medium. *$P < 0.05$ compared with that at 1 day ($n = 3$).

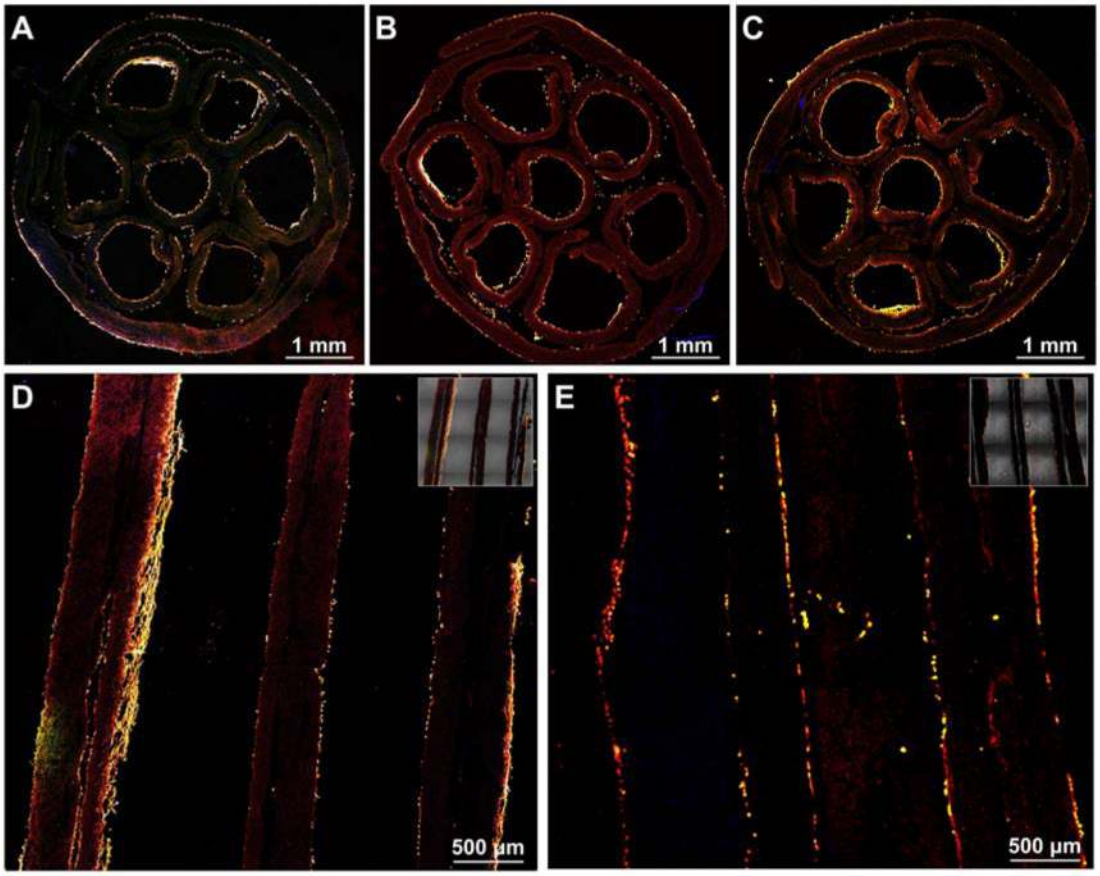

Figure 7.

Fluorescence micrographs of the derived cells showing the distribution of the derived cells in the multi-tubular conduit with a length of 4.2 cm. The conduit was frozen sectioned along the direction perpendicular to the longitudinal axis at the (A) proximal, (B) center, and (C) distal positions, and along the direction parallel to the longitudinal axis at the (D) center and (E) boundary areas, respectively. S100 was stained with Alexa Fluor 488 anti-S100 (green), F-actins were stained with Alexa Fluor 555 phalloidin (red), and the cell nuclei were stained with DAPI (blue), respectively. The inserted images at the top right corners in (D) and (E) are the overlay of fluorescence micrograph and the corresponding bright-field image.